NiCoPd inlaid NiCo-bimetallene for efficient electrocatalytic methanol oxidation

Long Zhao[a], *Ming Wen*[a,*], *Hao Fang*[a,b], *Kexin Meng*[a], *Xiaoyu Qiu*[a], *Qingsheng Wu*[a], *Yongqing Fu*[c]

[a] School of Chemical Science and Engineering, Shanghai Key Laboratory of Chemical Assessment and Sustainability, Tongji University, Shanghai, 200092, China

[b] School of Chemistry and Chemical Engineering, Shandong Provincial Key Laboratory of Molecular Engineering, Qilu University of Technology, Jinan, Shandong, 250353, China

[c] Faculty of Engineering and Environment, Northumbria University, Newcastle upon Tyne, NE1 8ST, UK

* Corresponding Authors: Ming Wen, E-mail: m_wen@tongji.edu.cn

Keywords: bimetallene, electrocatalysis, two-dimensional ultrathin materials, methanol oxidation, anti-CO poisoning

Abstract: Pd-based metallenes have attracted great attention recently as newly burgeoning two-dimensional (2D) materials, attributed to their significantly increased active surface areas and intrinsic electrocatalytic activities. Therefore, they could be used as a potential candidate as the high performance electrocatalyst for methanol oxidation reactions (MOR) in the direct methanol fuel cell. Herein, a new strategy is proposed to fabricate NiCoPd inlaid NiCo-bimetallene (NiCoPd/NiCo-bimetallene) by structure directing effect of 18-crown-6 ether under ultrasonic-pulse interface together with HCHO reduction and atom-diffusion-aging process. NiCoPd ternary-alloy with uniformly dispersed Pd active sites are decorated onto NiCo-bimetallenes, achieving remarkably enhancing the effective utilization of Pd atoms. What's more, the intrinsic activity is enhanced by the 'bifunctional mechanism' of NiCo-bimetallene adsorption of intermediate species and increased Pd active sites. Moreover, the anti-CO poisoning ability is optimized through 'alloying ligand effect' of NiCoPd. Therefore, the NiCoPd/NiCo-bimetallene exhibits excellent mass activity for MOR, which is higher than commercial Pd/C. This work suggests the new way of Pd-based metallenes catalyst approach to efficiently electrocatalytic MOR.

1. Introduction

Since the discovery of graphene in 2004,[1,2] it has been a hot research topic to search for graphene derived and other new types of two-dimensional (2D) materials (or called Xenes).[3,4] Among them, metallenes have recently attracted great attention in the field of direct methanol fuel cell (DMFC) as one of newly burgeoning 2D materials.[5] DMFC has the characteristics of high energy transition efficiency, convenient handling process, and environmental friendliness,[6] is considered as one of key advanced energy conversion and storage technologies to solve the rising energy demand.[7] Its performance is largely determined by the performance of anodic methanol oxidation reactions (MOR). Notably, Pd-based metallene catalysts have been proved as one of the best electrocatalysts for MOR, due to their excellent mass activity, such as Pd_3Pb metallene,[8] Pt-on-Pd dendritic metallene,[9] and porous Pd metallene.[10] However, the high cost and poor durability of these Pd-based metallene catalysts are the key obstacle for their commercial applications. In this regard, alloying Pd with other cheap transition metals can significantly reduce the cost. More importantly, Pd-based alloy catalyst, such as PdNi,[11] FePtPd,[12] CoPtPd,[13] CuFePd,[14] have further enhanced the anti-CO poisoning ability toward MOR, which is attributed to the following facts. The adsorption of hydroxyl intermediate (OH_{ads}) on transition metal groups (Ni, Bi, Ni, Cu, Co, and Sn) in Pd-based alloy can not only promote the oxidation of CO and -─CH_x species,[15-17] also release more active sites of Pd for electrocatalysis and provide oxygen sources for CO-like poisoning species, which are adsorbed on Pd to be transformed into CO_2.[18] What's more, the transition metals in the Pd-based alloy can regulate electron structures of Pd and reduce the adsorption energy between the toxic species and Pd surface.[19-22] However, from the perspective of structure, the smaller specific surface area of Pd-based alloy catalyst reported above will lead to lower utilization of active sites,[11-14] while the advantages of metallene structure in the following aspects are more obvious. The atomically thin structures endow them with ultrahigh surface-to-volume ratios, making it possible to expose great proportions of coordinatively unsaturated metal atoms at surface and edges which may become active centers to enhance catalyzing reaction.[23] The full exposure of active sites makes them readily functionalized, which is beneficial to enhance their stability, electronic structures, physicochemical properties, and thus final catalytic performance.[5,24] Compared with the non-metal elemental X-enes (e.g., phosphorene, silicone, and borophene), the large specific surface areas and improved surface energy of metal atoms can greatly promote the adsorption of reactants.[25] The higher connectivity of atoms can significantly reduce the charge

transfer distances, thus accelerating charge transfer during electrocatalysis process.[26] Metallenes can be formed in a freestanding format without supports, enabling their flexible applications.[27] Considering all above issues, the combination of Pd-based transition metal alloys and transition metal metallenes may be a strategy to solve the problems of high cost and poor durability of Pd-based catalysts for MOR.

Herein, a novel 2D heterostructure of NiCoPd inlaid NiCo-bimetallene (NiCoPd/NiCo-bimetallene) has been designed and synthesized through structure directing effect of 18-crown-6 ether under under ultrasonic-pulse interface together with HCHO reduction and atom-diffusion-aging process. The constructed NiCo-bimetallene can maximize the accessible surface areas, which facilitates the electrode/electrolyte contact and guarantees a high ion transfer and effective electron delivery in electrochemical catalytic reaction system. The HCHO reduction and atom-diffusion-aging process in the solvothermal system results in NiCoPd ternary-alloy are embedded in NiCo-bimetallene. In the case, Pd active sites in the NiCoPd ternary-alloy can be well dispersed on the surface of NiCo-bimetallene rather than in the interior, thus the availability of Pd sites can be substantially increased. In virtue of the enhanced intrinsic activity via the 'bifunctional mechanism', i.e. the adsorption of NiCo-bimetallene for intermediate species and the increased Pd active site. Moreover, the anti-CO poisoning ability can be optimized through 'alloying ligand effect' of NiCoPd ternary-alloy, since the electronic structure of Pd is adjusted to reduce the affinity of intermediate species. All above advantages enable the designed NiCoPd/NiCo-bimetallene to exhibit excellent catalytic performance for MOR with mass activity of 861 mA/mg_{Pd}, which is better than that of commercial Pd/C electrocatalyst. Meanwhile, the catalytic activity can be maintained after 4500 s. This design strategy and proposed material structure affords an approach to new efficient catalyst.

2. Experimental Section

2.1 Synthesis of NiCo-bimetallene

The NiCo-bimetallene was synthesized using two-phase solution method. The typical synthesis process is described as follows. $CoCl_2 \cdot 6H_2O$ pentanol solution (75 mL, 5 mM) and $NiCl_2 \cdot 6H_2O$ aqueous solution (25 mL, 5 mM) were mixed to form two-phase interfaces of pentanol and aqueous solution. Then $NaBH_4$ (10 mL, 3 *wt*.%) aqueous solution containing 18-crown-6 ether (1 g) was slowly added into the above two-phase interface under ultrasonic agitation. After 120 min reaction,

the product of NiCo-bimetallene was collected at two-phase interface. It should be noted that N_2 gas has been continuously introduced for protection during the whole synthesis process.

2.2 Synthesis of NiCoPd/NiCo-bimetallene

3 mL of as-obtained NiCo-bimetallene was added into EG (10 mL) solution. Then H_2PdCl_4 solution (1 mL, 5 mM) and HCHO (40%, 100 μL) were added into the above solution. The mixed solution was transferred to the autoclave and heated. Finally, powders were recovered, rinsed, and dried.

2.3 Characterization

Field-emission scanning electron microscope (FE-SEM, S-4800, Japan) was used to investigate the morphology of the samples, and elemental compositions were analyzed using an energy dispersive X-ray spectroscope (EDS), which was conducted at 20 keV on a TN5400 EDS instrument (Oxford). Microstructures of the materials were studied using a high-resolution transmission electron microscope (HR-TEM, JEM-2100EX, Japan). Spherical aberration corrected transmission electron microscope (AC-TEM, JEM ARM 200F, Japan) was used to measure HADDF image of element mapping under an accelerating voltage of 200 kV. Powder X-ray diffraction (XRD) patterns were obtained using a Bruker D8 (German) X-ray diffractometer with a Cu Kαradiation source (λ = 0.1541 nm) and a scanning angle (2θ) of 30°-80°, operated at 40 kV and 40 mA. Chemical states of elements were analyzed using an X-ray photoelectron spectroscope (XPS, RBD-upgraded PHI-5000C ESCA system, Perkin Elmer) with a Mg Kα radiation ($h\nu$ = 1486.6 eV). Before analyzing the XPS peaks, the binding energies of all the elements were calibrated using the containment carbon (C1s = 284.6 eV) as the reference. Deconvolution of the XPS spectra was performed after subtracting the background of each peak using the Shirley function.

2.4 Electrochemical measurements

Electrocatalytic performance of the as-prepared products was evaluated using a CHI 601E electro-chemistry workstation (Shanghai, China) with a three-electrode cell. Then, 5 μL of the 4 $mg \cdot mL^{-1}$ catalyst suspension was dropped on the glass carbon electrode. After the electrode was thoroughly dried, 1 μL of a 0.5 *wt*.% Nafion solution was cast onto the electrode surface to maintain the stability of the catalysts. Cyclic voltammetry (CV) measurements were performed in scan

range from 0 to -1 V *vs*. Hg/HgO at a sweep rate of 50 $mV \cdot s^{-1}$ in a nitrogen-saturated solution of 0.5 M KOH and 0.5 M KOH + 0.5 M methanol. The chronoamperometric curves were measured at constant potential of -0.2 V *vs*. Hg/HgO for 20000 s. The accelerated cycling tests were conducted for 500 cycles. For comparison, the commercial Pd/C catalyst (40 *wt*.%) was used as the benchmark, and the same procedure as described above was applied to conduct the electrochemical measurements.

3. Results and Discussion

3.1 Design and fabrication

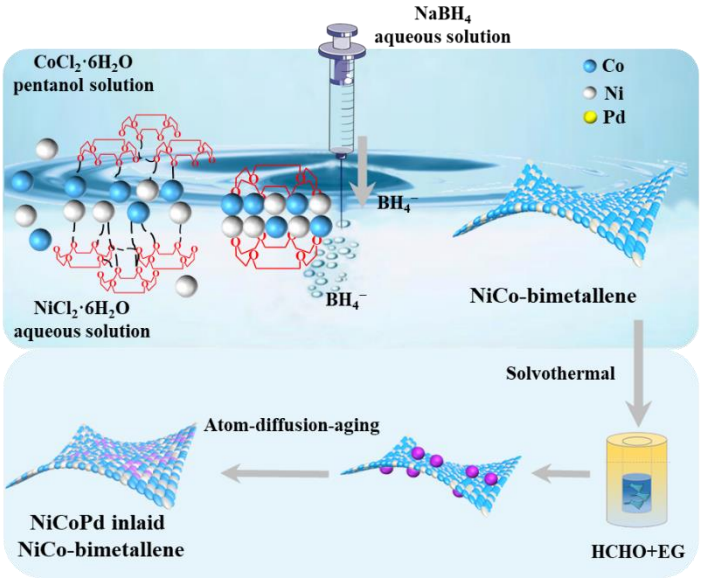

Figure 1. Synthesis schematic view of NiCoPd/NiCo-bimetallene.

A schematic view for the synthesis of NiCoPd/NiCo-bimetallene is illustrated in Figure 1. 18-crown-6 ether is selected as the structure directing agent for the construction of 2D NiCo-bimetallene. 18-crown-6 ether can shuttle continuously between pentanol and aqueous solution under the action of ultrasound agitation because it is a macrocyclic molecule containing hydrophilic ether groups and hydrophobic alkyl chains,[28] which makes the primary 18-crown-6 ether coordination complex of Ni(II)&Co(II) form at the interface of two-phase solution.[29,30] Since there are lone pair electrons in the ether oxygen of 18-crown-6 ether molecule, this primary complex may show a 2D arrangement at the two-phase interface.[31,32] With the subsequent dropwise addition of reducing agent of $NaBH_4$ aqueous, the primary 18-crown-6 ether coordination complex of Ni(II)&Co(II) is destroyed, which makes the metal ions released slowly and continuously. Under the synergistic effect of ultrasonic induced aggregation,[33] the reduced

metal atoms can still be arranged in two-dimensional space and alloyed with the help of high-energy pulse energy. Thus, the formation of 2D bimetallene structure is promoted (Figures S1-2). In the continuously solvothermal reaction process, Pd ions are slowly reduced by HCHO. Simultaneously, the lone pair electrons on oxygen in EG can act as a linker, which leads to the reduced Pd being adsorbed on the surface of NiCo-bimetallene. Further, the reduced Pd undergo uniformly slow atom-diffusion process and long-time aging treatment to form NiCoPd/NiCo-bimetallene finally.[34-36]

3.2. Morphologies and structures

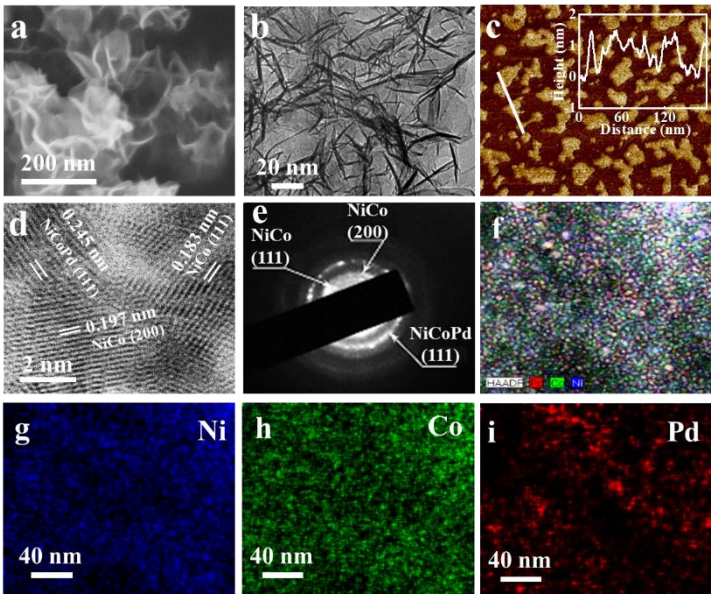

Figure 2. The SEM (a), TEM (b), AFM (c), HRTEM (d) images, SADP pattern (e), HADDF image (f) with element mapping (g-i) of NiCoPd/NiCo-bimetallene.

Figure 2 shows the morphology and structure of NiCoPd/NiCo-bimetallene. The SEM and TEM images reveal that the synthesized NiCoPd/NiCo-bimetallene has a 2D ultrathin structure within the NiCoPd ternary-alloy inlaid NiCo-bimetallene (Figures 2a-b). The thickness can be obtained from the AFM analysis, which is shown in Figure 2c. Compared with NiCo-bimetallene with thickness of 0.9 nm (Figures S3a-c), NiCoPd/NiCo-bimetallene has a much larger thicker thickness of 1.45 nm, mainly due to the diffusion of Pd into NiCo alloy in bimetallene to form NiCoPd ternary-alloy. In Figure 2d, the HRTEM image shows three different lattice spacings of 0.183, 0.197, and 0.245 nm, corresponding to NiCo (111), NiCo (200), and NiCoPd (111) planes, respectively. SADP pattern also confirms the formation heterostructures of NiCoPd inlaid NiCo-

bimetallene, which can be revealed by the polycrystalline diffraction rings of (111) & (200) planes of NiCo and (111) plane of NiCoPd (Figure 2e). There are two obvious changes which can be observed compared with NiCo-bimetallene which only shows NiCo (111) plane with a lattice spacing of 0.183 nm (Figure S3d). The elemental distributions of NiCoPd/NiCo-bimetallene were revealed by the HAADF-STEM-EDS mappings, where the combined (Figure 2f), Ni (Figure 2g), Co (Figure 2h), and Pd (Figure 2i) images reveal that Ni and Co elements are mainly uniform distributed, whereas distribution of Pd element is relatively concentrated due to the formation of NiCoPd ternary-alloy. Pd doesn't appear in the pure NiCo-bimetallene (Figure S4). We can confirm that the NiCoPd/NiCo-bimetallene heterostructure can be well achieved.

Figure 3a shows the XRD pattern of NiCo-bimetallene, which reveal the diffraction peaks at 44.3°, 51.6°, and 76.0°, corresponding to (111), (200), and (220) lattice planes (Ni-PDF#: 65-0380 and Co-PDF#: 15-0806). Obviously, the diffraction peaks of (111), (200), and (220) lattice planes are shifted to 42.4°, 49.4°, and 72.1° when the NiCoPd ternary-alloy are produced by HCHO reduction process and atom-diffusion-aging in the solvothermal system. These peaks are located between those of NiCo alloy and crystal Pd (PDF#: 65-6714), confirming the formation of NiCoPd ternary-alloy. EDS analysis confirms that Pd exists in the NiCoPd/NiCo-bimetallene but is absent in NiCo-bimetallene, which is consist with the above XRD results (Figure 3b). XPS results are used to provide evidence for the reconfiguration of electron structure of NiCoPd/NiCo-bimetallene. The survey spectrum of NiCoPd/NiCo-bimetallene reveals peaks of Ni 2p, Co 2p, and Pd 3d (Figure 3c). The high-resolution XPS spectrum of Ni 2p is shown in Figure 3d. After the HCHO reduction and atom-diffusion-aging process, the binding energy shows Ni^0 in NiCo-bimetallene is shifted to high binding energy (~1.1 eV) from 852.3 and 870.3 eV to 853.4 and 871.3 eV for Ni $2p_{3/2}$ and Ni $2p_{1/2}$, respectively.[37,38] The similar shifts for Co 2p (~0.9 eV), which are from 778.40 to 779.30 eV (Co $2p_{3/2}$) and from 794.00 to 794.9 eV (Co $2p_{1/2}$) (Figure 3e).[37,38] However, for the characteristic peaks of Pd 3d in NiCoPd/NiCo-bimetallene shift toward a lower binding energy side with a value of ~ 0.80 eV, e.g., from 334.90 to 334.1 eV (Pd $3d_{5/2}$), and from 340.10 eV to 339.30 eV (Pd $3d_{3/2}$) (Figure 3f).[39,40] The reason for the above phenomenon is that the different electronegativities of the metals lead to effective electron transfer between metals in the alloy system, which results in the shift of the binding energy peak position in the XPS spectra. The characteristic peaks shift to higher binding energy orientations when the metals donate electrons to the others, whereas they would shift to a lower orientation when receiving electrons.[41]

When the atom-diffusion-aging is finally carried out to form NiCoPd ternary-alloy, Pd receives electrons from Ni and Co, which leads to the left-shift. The observed changing trends of XPS peaks are consistent with the prediction ones from HRTEM and XRD analysis results. All these prove the formation of NiCoPd/NiCo-bimetallene.

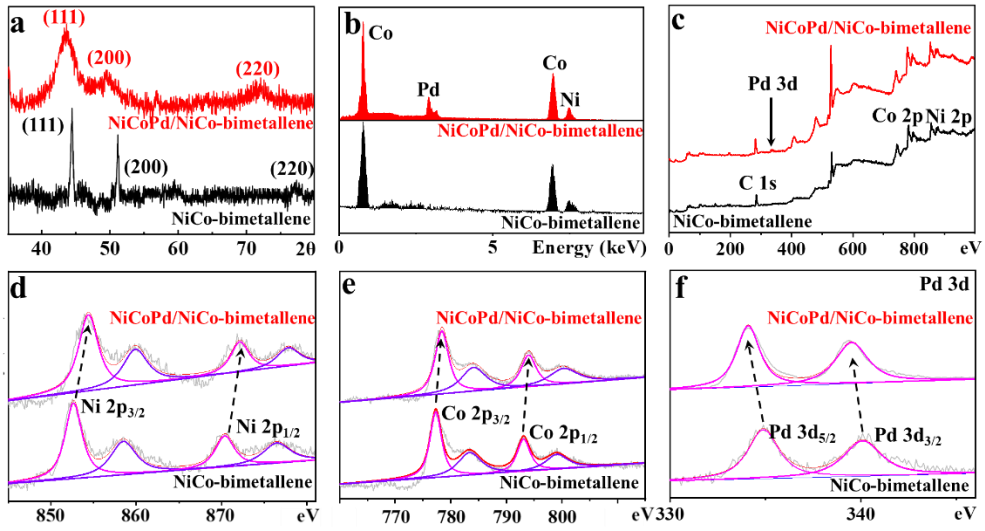

Figure 3. XRD patterns (a), EDS spectra (b), Full XPS survey spectra scans (c), and element detail XPS spectra (d-f) of NiCoPd/NiCo-bimetallene and NiCo-bimetallene, respectively.

3.3. Catalytic activity of MOR

MOR in an alkaline media is selected as the probe reaction to investigate the catalytic performance of NiCoPd/NiCo-bimetallene. In contrast to the acid environment, an alkaline media can provide a less corrosive environment to the catalysts,[42] and the abundant OH^- in the alkaline media provide the sources of OH_{ads}, thus improving the reaction speed of the oxidation step of methanol and CO intermediates.[43,44] The catalytic performance of MOR is evaluated via assessing its mass activity, electrochemical active surface area (EASA), anti-CO poisoning ability, and stability. Considering that the importance of active Pd distribution in formed NiCoPd ternary-alloy is affected by aging time and temperature, these two parameters are investigated first. In the solution of 0.5 M KOH + 0.5 M methanol at 25°C, CV curves of NiCoPd/NiCo-bimetallene obtained in different atom-diffusion-aging times (Figure 4a**)** and temperatures (Figure 4b) are quite similar and both display two characteristic anodic (oxidation) current peaks. The oxidation peak in the forward scan is corresponding to the oxidation of freshly chemisorbed species coming from methanol adsorption, meanwhile the reverse oxidation peak is primarily associated with the removal of incompletely oxidized carbonaceous species (e.g., CO, HCOO, etc.) in the forward

scan.[45] For comparisons of electrochemical activity, Table 1 lists the values of the forward and reverse oxidation current peaks for MOR.

Table 1. Information of electrocatalytic activity by NiCoPd/NiCo-bimetallene toward MOR.

Materials		Forward sweep	Reverse sweep	I_f/I_b	EASA
		I_f (mA/mg$_{Pd}$)	I_b (mA/mg$_{Pd}$)		(m^2/g $_{Pd}$)
Aging time (h)	24	665	515	1.29	134.1
	48	861	687	1.25	185.2
	72	705	616	1.14	151.8
Aging temperature (°C)	120	756	636	1.19	165.2
	150	861	687	1.25	185.2
	180	668	512	1.30	149.1
Mass ratio of Ni:Co:Pd	0:90:10	720	605	1.19	151.6
	27:63:10	861	687	1.25	185.2
	45:45:10	755	659	1.15	172.8
	63:27:10	640	621	1.03	116.1
	0:90:10	547	524	1.04	104.9
	27:63:3	679	525	1.29	126.1
	27:63:10	861	687	1.25	185.2
	27:63:15	810	883	0.91	100.5
NiCo-bimetallene		224	161	1.39	——
Commercial Pd/C		450	611	0.74	58.6

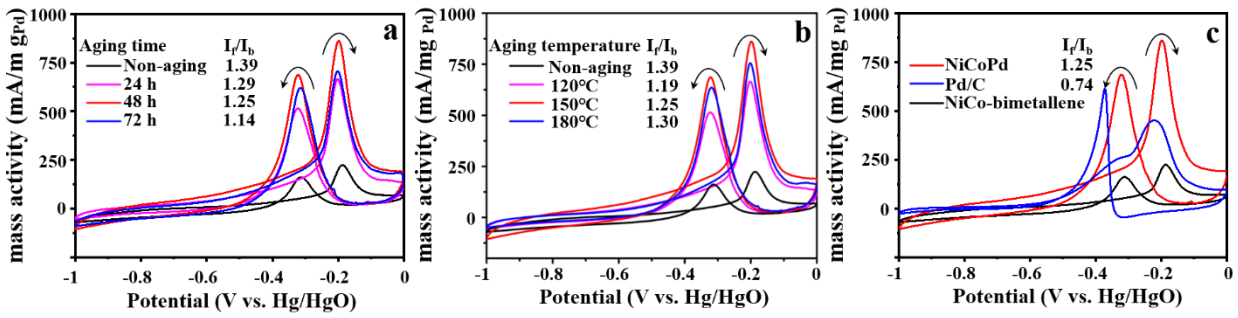

Figure 4. CV curves of the prepared samples obtained in different conditions (sweep rate of 50 $mV \cdot s^{-1}$ in 0.5 M KOH + 0.5 M methanol solution): atom-diffusion-aging times (a) and temperatures (b), comparison materials (c).

It is clearly seen that the NiCoPd/NiCo-bimetallene shows a much higher catalytic activity than that of NiCo-bimetallene (non-aging treatment), indicating the electrocatalytic activity attributed to NiCoPd nanophase. In addition, the mass activity of NiCoPd/NiCo-bimetallene for MOR exhibits substantial changes under different atom-diffusion-aging conditions. The mass activity reaches a maximum value of 861 mA/mg_{Pd} under 150℃ for 48 h, which shows its larger value compared with that of the commercial Pt/C catalyst (i.e., 450 mA/mg_{Pd}). This is mainly attributed to the influence of atom-diffusion-aging treatment on the EASA. To verify this, the EASA of the electrodes are calculated by the following equation:[46]

$$EASA = Q/(405 \times [Pd]) \quad (1)$$

where [Pd] represents the Pd loading (mg/cm^2). The determining the coulombic charge (Q) corresponds to the reduction peak of palladium oxide in CV curves of sample in 0.5 M KOH solution.[47] A charge value of 405 $\mu C/cm^2$ is assumed for the reduction of PdO monolayer.[48]

In the process of aging treatment, the influencing factors of EASA depend on the morphology of 2D structure of NiCo-bimetallene and alloying degree of NiCoPd. As expected, the calculation results of EASA based on the Figure S5 show that the maximum EASA value (185.2 m^2/g Pd) can be obtained by the atom-diffusion-aging treatment under 150℃ for 48 h, which is corresponding to the conditions for the optimal mass activity (Table 1). In theory, the degree of atomic interdiffusion has been enhanced when the temperature and duration are increased, which is conducive to the alloying of reduced Pd and NiCo-bimetallene. However, the EASA value does not increase but it becomes decreased with the increase of atom-diffusion-aging treatment time and temperature. There are two reasons to this phenomenon. The first one is that the agglomeration

of 2D bimetallene structure leads to the decrease of EASA and the number of active sites (Figures S6 and S7). The second one is that the excessive atom-diffusion-aging treatment causes migration of some platinum atoms into the interior of NiCo-bimetallene rather than staying at the surface. Therefore, these platinum atoms are no longer the catalytic active centers, thus resulting in the decrease of ECSA. As a higher EASA value is the key to ensure a higher mass activity, therefore, the mass activity of optimized NiCoPd/NiCo-bimetallene is much higher than that of the commercial Pd/C (450 mA/mg_{Pd}) due to its larger EASA (Figures 4c and S8, Table1). Compared to Pd/C, the anti-CO poisoning ability of NiCoPd/NiCo-bimetallene in the process of catalytic MOR is enhanced by the 'bifunctional mechanism'. Specifically, the NiCo-bimetallene can facilitate the oxidation process and the removal of the CO intermediates adsorbed onto the NiCoPd ternary-alloy active sites by adsorbing hydroxide (OH^-) species.[49] Consequently, more NiCoPd ternary-alloy active sites become accessible for the MOR, thereby enhancing catalytic performance to obtain a higher mass activity.[50] In the process of MOR, large numbers of CO intermediates (CO_{ads}) have been produced, and then adsorbed on the surfaces of the catalyst. They occupy the active sites, thus causing the inactivation or partially inactivation of catalyst.[51] The anti-CO poisoning ability of catalyst is an important part of evaluating the catalytic activity and catalytic efficiency.[52] The ratio of the forward oxidation current density (I_f) to the reverse oxidation current density (I_b), (I_f/I_b), can be used to describe the anti-CO poisoning ability of the catalyst.[53] A high I_f/I_b ratio suggests efficient electrooxidation of methanol during the forward scan and less accumulation of residues on the electrodes, whereas a low ratio indicates incomplete electrooxidation of methanol and excessive accumulation of carbonaceous residues on the electrode surface.[53-55] According to Table 1, the values of I_f/I_b for all the NiCoPd/NiCo-bimetallene are higher than that of commercial Pd/C, which proves their excellent anti-CO poisoning ability. The electrochemical reactions are listed as follows:

$$NiCoPd + CH_3OH + 4OH^- \rightarrow CO_{ads}\text{-}NiCoPd\text{-}CO_{ads} + 4H_2O + 4e^- \quad (2)$$

$$NiCo + OH^- \rightarrow OH_{ads}\text{-}NiCo\text{-}OH_{ads} + e^- \quad (3)$$

$$CO_{ads}\text{-}NiCoPd\text{-}CO_{ads} + OH_{ads}\text{-}NiCo\text{-}OH_{ads} \rightarrow (COOH)_{ads}\text{-}NiCoPd\text{-}(COOH)_{ads} + NiCo \quad (4)$$

$$(COOH)_{ads}\text{-}NiCoPd\text{-}(COOH)_{ads} + OH^- \rightarrow NiCoPd + CO_2\uparrow + H_2O + e^- \quad (5)$$

It is clear from the above MOR process that NiCoPd is the main MOR catalytic active site. Methanol is oxidized to CO_{ads} after adsorption. Subsequently, the adsorbed OH species by NiCo-bimetallic around the NiCoPd can promote the further oxidation of CO_{ads} to the final product CO_2

at the NiCoPd active site, as shown in Figure 5a. Theoretically, adsorbed CO intermediates bind strongly to the Pd sites,[34] but for NiCoPd ternary-alloy, the inherent structural coupling between the NiCo lattice and the Pd lattice generates a compression strain of the Pd lattice, mainly due to the shorter interatomic distance of the NiCo sites as compared with that of Pd. Therefore, this so-called 'alloying ligand effect' increases the d-orbital overlap, contributing to a down-shift in energy for the weighted center of the d-band.[56] In essence, electron density is withdrawn from the Pd d-band towards that of the dopant metals. In terms of practical consequences for catalysis, both the lower weighted center of the d-band and the reduced electron density collectively contribute to a lowered CO affinity as a result of a concomitant weakening of the overlap between the Pd d-orbitals and the CO π*-orbitals.[57] Hence, CO coverage is effectively reduced, which correspondingly increases the number of exposed Pd active sites available for the MOR. In terms of the influence of Ni:Co mass ratio (Figure 5b), the reported DFT calculations[58] had been certified that the adsorption energies (E_{ads}) of methanol on the Ni sites is higher than that of on the Co sites, which shows the preferential adsorption of methanol molecules on the Ni sites. The higher values of E_{ads} imply a higher degree of methanol poisoning. On the other hand, the adsorption energy of CO on Ni sites is also higher than that on the Co sites, which results in a higher CO poisoning on that on the Ni sites. For the influence of Pd mass ratio (Figure 5c), the mass activity of MOR is gradually increased with the increase of the mass ratio of Pd. It is worth noting that this ratio is unable to increase indefinitely. When the ratio is increased to 15%, the value of I_f/I_b is decreased rapidly to 0.91, indicating the decline of the anti-CO poisoning ability of the catalyst. Therefore, the maximum EASA value and optimal mass activity are obtained when the mass ratio of Ni:Co:Pd in NiCoPd/NiCo-bimetallene is 27:63:10 (Figure S9).

The catalytic stability is a crucial index for a comprehensive evaluation of the electrocatalyst for a fuel cell. In this work, the following two aspects are discussed about its the stability, i.e., the retention current after chronoamperometry test, and the structural stability after 500 CV cycles. Results indicate that the as-prepared NiCoPd/NiCo-bimetallene show a better desirable stability in each of the above two aspects. Figure 5d illustrates the chronoamperometric curves at a constant potential of -0.2 V *vs*. Hg/HgO for 20000 s. During this period, the optimized NiCoPd/NiCo-bimetallene retains a maximum of 454.6 mA/mg_{Pd} until the stability is reached. This result is superior to the known metallenes (Table S1). This value is much higher than those of NiCo-bimetallene and commercial Pd/C. Figure 5e compares the mass activities of optimized

NiCoPd/NiCo-bimetallene before and after 500 CV cycles, which shows that the mass activity of the one after 500 CV cycles decreases by about 50%, the I_f/I_b value is close to 1, and the morphology of 2D bimetallene is also changed significantly. This may be due to the irreversible phase transformation of the alloy phase caused by the adsorption of intermediate species in the MOR process (Figure S10). This results in the weakened bonding energy of NiCoPd/NiCo-bimetallene, therefore, it is difficult to maintain the metallene structure.[59,60]

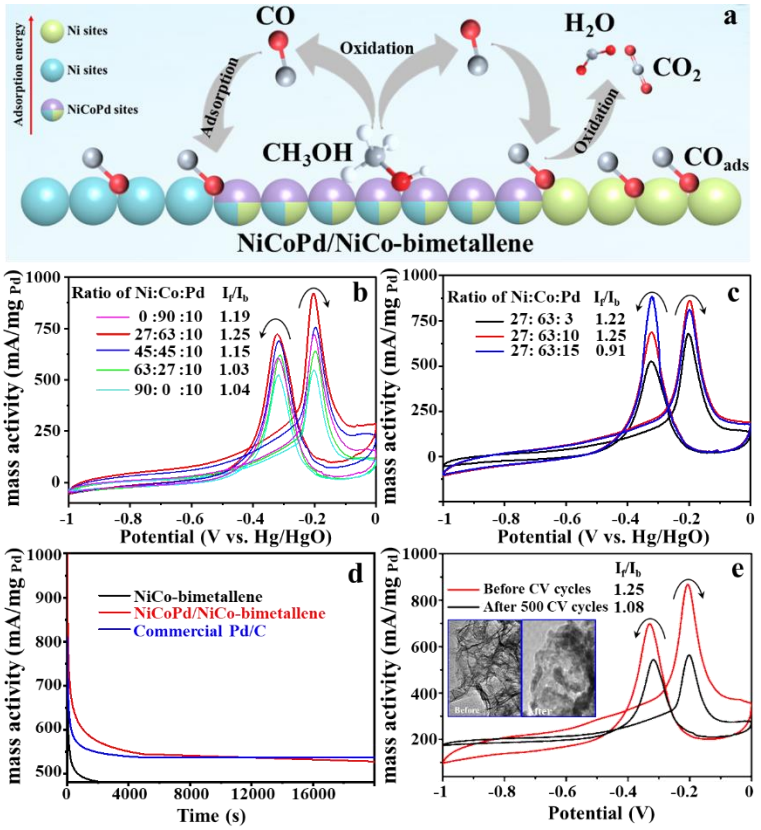

Figure 5. Schematic diagram of MOR electrocatalytic mechanism NiCoPd/NiCo-bimetallene catalyzed (a), CV curves of Ni:Co:Pd mass ratio (b-c) at sweep rate of 50 $mV \cdot s^{-1}$ in 0.5 M KOH + 0.5 M methanol solution, stability tested using chronopotentiometry (d), mass activity (e, TEM images illustration) of before and after CV cyclic.

4. Conclusion

In summary, based on the structure directing effect of 18-crown-6 ether under ultrasonic-pulse interface together with the HCHO reduction and atom-diffusion-aging process in solvothermal system, a novel 2D heterostructure of NiCoPd/NiCo-bimetallene has been successfully synthesized. The MOR is selected to verify the electrocatalytic activities of NiCoPd/NiCo-

bimetallene. The intrinsic activity and anti-CO poisoning ability can be remarkably enhanced via the 'bifunctional mechanism' and 'alloying ligand effect' between inlaid NiCoPd tenary-alloy nanophase and NiCo-bimetallene. By virtue of the maximize utilization of Pd active sites on NiCo-bimetallene, the optimized NiCoPd/NiCo-bimetallene with Ni:Co:Pd ratio of 27:63:10 exhibits excellent catalytic performance, which is better than commercial Pd/C electrocatalyst. This work explores the new way approach to the ternary-alloy included metallene for high efficiency catalysis system toward MOR in DMFC and others.

Supporting Information

Description of reagents used, figures of SEM images, TEM images, AFM images, XRD patterns, EDS patterns, FTIR spectrum, CV curves, and table of comparisons of MOR performance (Text S1, Figure S1-S10, and Table S1).

Author Contributions

Long Zhao: Writing-Original draft preparation, Investigation, Performances tests. The lead of contribution. **Ming Wen:** Conceptualization, Writing-Reviewing and Editing, Funding acquisition. The lead of contribution. **Hao Fang:** Investigation. The supporting of contribution. **Kexin Meng:** Material preparation. The supporting of contribution. **Xiaoyu Qiu:** Material preparation. The supporting of contribution. **Qingsheng Wu:** Conceptualization, Writing-Reviewing and Editing. The supporting of contribution. **Yongqing Fu:** Writing-Reviewing, Funding acquisition. The supporting of contribution.

Funding Sources

This work was financially supported by the National Natural Science Foundation (NSFC Nos: 22171212), Science and Technology Committee of Shanghai Municipality (21160710300, 19DZ2271500) by China, International Exchange Grant (IEC/NSFC/201078) through Royal Society UK and NSFC.

Notes

The authors declare that they have no known competing financial interests or personal relationships that could have appeared to influence the work reported in this paper.

References

(1) Chakraborty, G.; Park, I. H.; Medishetty, R.; Vittal, J. J. Two-dimensional Metalorganic Framework Materials: Synthesis, Structures, Properties and Applications. *Chem. Rev.* **2021**, *121*, 3751-3891.

(2) Deng, D. H. Bimetallene Advances Oxygen Electrocatalysis. *Sci. China Chem.* **2020**, *63*, 147-148.

(3) Fu, G. T.; Yan, X. X.; Chen, Y. F.; Xu, L.; Sun, D. M.; Lee, J. M.; Tang Y. W. Boosting Bifunctional Oxygen Electrocatalysis with 3D Graphene Aerogel-Supported Ni/MnO Particles. *Adv.Mater.* **2018**, *30*, 1704609.

(4) Wang, H.; Li, J. M.; Li, K.; Lin, Y. P.; Chen, J. M.; Gao, L. J.; Nicolosi, V.; Xiao, X.; Lee, J. M. Transition metal nitrides for electrochemicalenergy applications. *Chem. Soc. Rev.* **2021**, *50*, 1354-1390.

(5) Prabhu, P.; Lee, J. M. Metallenes as Functional Materials in Electrocatalysis, *Chem. Soc. Rev.* **2021**, *50*, 6700-6719.

(6) Cheng, H.; Gui, R. J.; Liu, S.; Xie, Y.; Wu, C. Z. Local Structure Engineering for Active Sites in Fuel Cell Electrocatalysts. *Sci. China Chem.* **2020**, *63*, 1543-1556.

(7) Hui, L.; Zhang, X. T.; Xue, Y. R.; Chen, X.; Fang, Y.; Xing, C. Y.; Liu, Y. X.; Zheng, X. C. Du, Y. C.; Zhang, C.; He, F.; Li, Y. L. Highly Dispersed Platinum Chlorine Atoms Anchored on Gold Quantum Dots for a Highly Efficient Electrocatalyst. *J. Am. Chem. Soc.* **2022**, *144*, 1921-1928.

(8) Bu, L.; Tang, C.; Shao, Q.; Zhu, X.; Huang, X. Three-dimensional Pd_3Pb Nanosheet Assemblies: High-Performance Non-Pt Electrocatalysts for Bifunctional Fuel Cell Reactions. *ACS Catal.* **2018**, *8*, 4569-4575.

(9) Peng, X.; Lu, D.; Qin, Y.; Li, M.; Guo, Y.; Guo, S. Pt-on-Pd Dendritic Nanosheets with Enhanced Bifunctional Fuel Cell Catalytic Performance. *ACS Appl. Mater. Interfaces* **2020**, *12*, 30336-30342.

(10) Liu, Z.; Yang, X.; Lu, B.; Shi, Z.; Sun, D.; Xu, L.; Tang, Y.; Sun, S. Delicate Topotactic Conversion of Coordination Polymers to Pd Porous Nanosheets for High Efficiency Electrocatalysis. *Appl. Catal. B Environ.* **2019**, *243*, 86-93.

(11) Xu, C. X.; Liu, Y. Q.; Hao, Q.; Duan, H. M. Nanoporous PdNi Alloys as Highly Active and Methanol Tolerant Electrocatalysts towards Oxygen Reduction Reaction. *J. Mater. Chem. A* **2013**, *1*, 13542-13548.

(12) Zan, G. T.; Wu, T.; Zhu, F.; He, P. F.; Cheng, Y. P.; Chai, S. S.; Wang, Y.; Huang, X. F.; Zhang, W. X.; Wan, Y.; Peng, X. J.; Wu, Q. S. A Biomimetic Conductive Super-foldable Material. *Matter* **2021**, *4*, 3232-3247.

(13) Aricò, A. S.; Stassi, A.; D′Urso, C.; Sebastián, D.; Baglio, V. Synthesis of Pd_3Co_1@Pt/C Core-Shell Catalysts for Methanol-Tolerant Cathodes of Direct Methanol Fuel Cells. *Chem. Eur. J.* **2014**, *20*, 10679-10684.

(14) Zhang, X.; Zhang, Y. C.; Zhang, J. W.; Zhang, B. Anchoring Ternary CuFePd Nanocatalysts on Reduced Graphene Oxide to Improve the Electrocatalytic Activity for the Methanol Oxidation Reaction. *RSC Adv.* **2015**, *5*, 101563-101568.

(15) Yuan, X. L.; Zhang, Y.; Cao, M. H.; Zhou, T.; Jiang, X. J.; Chen, J. X.; Lyu, F. L.; Xu, Y.; Luo, J.; Zhang, Q.; Yin, Y. D. $Bi(OH)_3$/PdBi Composite Nanochains as Highly Active and Durable Electrocatalysts for Ethanol Oxidation. *Nano Lett.* **2019**, *19*, 4752-4759.

(16) Zhang, Z. Q.; Wu, Q.; Mao, K.; Chen, Y. G.; Du, L. Y.; Bu, Y. F.; Zhuo, O.; Yang, L. J.; Wang, X. Z.; Hu, Z. Efficient Ternary Synergism of Platinum/tin Oxide/nitrogen-doped Carbon Leading to High-Performance Ethanol Oxidation. *ACS Catal.* **2018**, *8*, 8477-8483.

(17) Chen, Z. L.; Liu, Y. W.; Liu, C.; Zhang, J. F.; Chen, Y. N.; Hu, W. B.; Deng, Y. D. Engineering the Metal/Oxide Interface of Pd Nanowire@CuO_x Electrocatalysts for Efficient Alcohol Oxidation Reaction. Small **2020**, *16*, 1904964.

(18) Xu, C. W.; Tian, Z. Q.; Shen, P. K.; Jiang, S. P. Oxide (CeO_2, NiO, Co_3O_4 and Mn_3O_4)-Promoted Pd/C Electrocatalysts for Alcohol Electrooxidation in Alkaline Media. *Electrochim. Acta* **2008**, *53*, 2610-2618.

(19) Chang, Q. W.; Kattel, S.; Li, X.; Liang, Z. X.; Tackett, B. M.; Denny, S. R.; Zhang, P.; Su, D.; Chen, J. G.; Chen, Z. Enhancing C-C bond Scission for Efficient Ethanol Oxidation using PtIr Nanocube Electrocatalysts. *ACS Catal.* **2019**, *9*, 7618-7625.

(20) Liu, J. F.; Luo, Z. S.; Li, J. S.; Yu, X. T.; Llorca, J.; Nasiou, D.; Arbiol, J.; Meyns, M.; Cabot, A. Graphene-supported Palladium Phosphide PdP_2 Nanocrystals for Ethanol Electrooxidation. *Appl. Catal. B Environ.* **2019**, *242*, 258-266.

(21) Shakibi Nia, N.; Guillén-Villafuerte, O.; Griesser, C.; Manning, G.; Kunze-Liebhäuser, J.; Arévalo, C.; Pastor, E.; García, G. W_2C-supported PtAuSn—a Catalyst with the Earliest Ethanol Oxidation Onset Potential and the Highest Ethanol Conversion Efficiency to CO_2 Known Till Date. *ACS Catal.* **2019**, *10*, 1113-1122.

(22) Lv, H.; Wang, Y.; Lopes, A.; Xu, D. D.; Liu, B. Ultrathin PdAg Single-Crystalline Nanowires Enhance Ethanol Oxidation Electrocatalysis. *Appl. Catal. B Environ.* **2019**, *249*, 116-125.

(23) Cao, C.; Ma, D. D.; Gu, J. F.; Xie, X.; Zeng, G.; Li, X.; Han, S. G.; Zhu, Q. L.; Wu, X. T.; Xu, Q. Metal-organic Layers Leading to Atomically Thin Bismuthene for Efficient Carbon Dioxide Electroreduction to Liquid Fuel. *Angew. Chem. Int. Ed.* **2020**, *59*, 15014-15020.

(24) Wang, H.; Chen, J. M..; Lin, Y. P.; Wang, X. H.; Li, J. M.; Li, Y.; Gao, L. J.; Zhang, L. B.; Chao, D. L.; Xiao, X.; Lee, J. M. Electronic Modulation of Non-van der Waals 2D Electrocatalysts for Efficient Energy Conversion. *Adv. Mater.* **2021**, *33*, 2008422.

(25) Li, Z.; Zhai, L.; Ge, Y.; Huang, Z.; Shi, Z.; Liu, J.; Zhai, W.; Liang, J.; Zhang, H. Wetchemical Synthesis of Two-Dimensional Metal Nanomaterials for Electrocatalysis. *Nat. Sci. Rev.* **2021**, *https://doi.org/10.1093/nsr/nwab142*.

(26) Gao, S.; Lin, Y.; Jiao, X.; Sun, Y.; Luo, Q.; Zhang, W.; Li, D.; Yang, J.; Xie, Y. Partially Oxidized Atomic Cobalt Layers for Carbon Dioxide Electroreduction to Liquid Fuel. *Nature* **2016**, *529*, 68-71.

(27) Cao, C. S.; Xu, Q.; Zhu, Q. L. Ultrathin Two-Dimensional Metallenes for Heterogeneous Catalysis. *Chem Catal.* **2022**, *2*, 1-31.

(28) Hazra, D. K.; Mukherjee, M.; Sen, R.; Saha, D.; Koner, S.; Mukherjee, A. K. 18-Crown-6 Ether Templated Transition-Metal Dicyanamido Complexes: Synthesis, Structural Characterization and DFT Studies. *J. Mol. Struct.* **2013**, *1033*, 137-144.

(29) Chen, S. Y.; Chen, J. C.; Qu, T. T.; Xiang, K.; Zhang, Y.; Hao, P. P.; Peng, L. M.; Xie, M. J.; Guo, X. F.; Ding, W. P. Crown ether induced assembly to γ-Al_2O_3 nanosheets with Rich Pentacoordinate Al^{3+} Sites and High Ethanol Dehydration Activity. *Appl. Surf. Sci.* **2018**, *457*, 626-632.

(30) Izatt, R. M.; Terry, R. E.; Haymore, B. L.; Hansen, L. D.; Dalley, N. K.; Avondet, A. G.; Christensen, J. J. Calorimetric Titration Study of the Interaction of Several Uni- and Bivalent Cations with 15-crown-5, 18-crown-6, and Two Isomers of Dicyclohexo-18-crown-6 in Aqueous Solution at 25°C and μ = 0.1. *J. Am. Chem. Soc.* **1976**, *98*, 7620-7626.

(31) Kafashi, S.; Yaftian, M. R.; Zamani, A. A. Binding Ability of Crown Ethers Towards Pb(II) Ions in Binary Water/Organic Solvents using Solvent Extraction Method. *J. Solution Chem.* **2015**, *44*, 1798-1811.

(32) Naseer, R.; Sankar Mal, S.; Kortz, U.; Armstrong, G.; Laffir, F.; Dickinson, C.; Vagin, M.;

McCormac, T. Electrocatalysis by Crown-Type Polyoxometalates Multi-Substituted by Transition Metal Ions; Comparative Study. *Electrochim. Acta* **2015**, *176*, 1248-1255.
(33) Yu, C. L., Yu, J. C. Sonochemical Fabrication, Characterization and Photocatalytic Properties of Ag/$ZnWO_4$ Nanorod Catalyst. *Mater. Sci. Eng. B* **2009**, *164*, 16-22.
(34) Poerwoprajitno, A. R.; Gloag, L.; Watt, J.; Cheong, S.; Tan, X.; Lei, H.; Tahini, H. A.; Henson, A.; Subhash, B.; Bedford, N. M.; Miller, B. K.; Peter B.; O'Mara, P. B.; Benedetti, T. M.; Huber, D. L.; Zhang,W. H.; Smith, S. C.; Gooding, J. J.; Schuhmann, W.; Tilley, R. D. A Single-Pt-Atom-on-Ru-Nanoparticle Electrocatalyst for CO-resilient methanol oxidation. *Nat. Catal.* **2022**, *5*, 231-237.
(35) Dumitraschkewitz, P.; Uggowitzer, P. J.; Gerstl, S. S. A.; Löffler, J. F.; Pogatscher, S. Size-Dependent Diffusion Controls Natural Aging in Aluminium Alloys. Nat. Commun. **2019**, *10*, 4746.
(36) Fukuda, Y.; Kado, Y.; Yoshikawa, T.; Oishi, K.; Mae, Y. Diffusion Distances of the Constituent Atoms in the Metallurgical Phenomena such as Recovery, Recrystallization, Grain Growth, and Aging in Aluminum and Copper Alloys. J. Mater. Eng. Perform. **2002**, *11*, 544-550.
(37) Li, Z. Y.; Li, J. F.; Jiang, K. H.; Yuan, S. Y.; Yu, D. K.; Wei, H.; Shi, Z. M.; Li, X. T.; Chu, H. B. PdCoNi Alloy Nanoparticles Decorated, Nitrogen-Doped Carbon Nanotubes for Highly Active and Durable Oxygen Reduction Electrocatalysis. *Chem. Eng. J.* **2021**, *411*, 128527.
(38) Gao, D.; Guo, J. N.; He, H. C.; Xiao, P.; Zhang, Y. H. Geometric and Electronic Modulation of fcc NiCo Alloy by Group-VIB Metal Doping to Accelerate Hydrogen Evolution Reaction in Acidic and Alkaline Media. *Chem. Eng. J.* **2022**, *430*, 133110.
(39) Pan, Y.; Zhu, Y. H.; Shen, J. H.; Chen, Y.; Li, C. Z. Carbon-loaded Ultrafine Fully Crystalline Phase Palladium-Based Nanoalloy PdCoNi/C: Facile Synthesis and High Activity for Formic Acid Oxidation. *Nanoscale* **2019**, *11*, 17334-17339.
(40) Zhao, Y. P.; Tao, L.; Dang, W.; Wang, L. L.; Xia, M. R.; Wang, B.; Liu, M. M.; Gao, F. M.; Zhang, J. J.; Zhao, Y. F. High-indexed PtNi Alloy Skin Spiraled on Pd Nanowires for Highly Efficient Oxygen Reduction Reaction Catalysis. *Small* **2019**, *15*, 1900288.
(41) Martins, M.; Metin, Ö.; Šljukić, B.; Sevim, M.; Sequeira, C.; Santos, D. PdNi Alloy Nanoparticles Assembled on Cobalt Ferrite-Carbon Black Composite as a Fuel Cell Catalyst. *Int. J. Hydrogen Energy* **2019**, *44*, 14193-14200.
(42) Zhao, X.; Li, X. Y.; An, L. L.; Iputera, K.; Zhu, J.; Gao, P. F.; Liu, R. S.; Peng, Z. M.; Yang, J.L.; Wang, D. L. Nitrogen-inserted Nickel Nanosheets with Controlled Orbital Hybridization and

Strain Fields for Boosted Hydrogen Oxidation in Alkaline Electrolytes. *Energy Environ. Sci.* **2022**, *15*, 1234-1242.

(43) Liu, J. P.; Ye, J. Q.; Xu, C. W.; Jiang, S. P.; Tong, Y. X. Kinetics of Ethanol Electrooxidation at Pd Electrodeposited on Ti. *Electrochem. Commun.* **2007**, *9*, 2334-2339.

(44) Huang, H. Y.; Chen, P. Y. Voltammetric Behavior of Pd(II) and Ni(II) Ions and Electrodeposition of PdNi Bimetal in N-butyl-N-methylpyrrolidinium Dicyanamide Ionic Liquid. *Electrochim. Acta* **2011**, *56*, 2336-2343.

(45) Hui, L.; Xue, Y. R.; Xing, C. Y.; Liu, Y. X.; Du, Y. C.; Fang, Y.; Yu, H. D.; Zhang, C.; He, F.; Li, Y. L. Atomic Alloys of Nickel-Platinum on Carbon Network for Methanol Oxidation. *Nano Energy* **2022**, *95*, 106984.

(46) Ye, N.; Zhao, P. C.; Qi, X. Y.; Sheng, W. C.; Jiang, Z.; Fang, T. Understanding the High Performance of PdSn-TaN(tantalum nitride)/C Electrocatalysts for the Methanol Oxidation Reaction: Coupling Nitrides and Oxophilic Elements. *J. Mater. Chem. A* **2022**, *10*, 266-287.

(47) Qin, Y. H.; Yang, H. H.; Zhang, X. S.; Li, P.; Ma, C. A. Effect of Carbon Nanofibers Microstructure on Electrocatalytic Activities of Pd Electrocatalysts for Ethanol Oxidation in Alkaline Medium. *Int. J. Hydrogen Energy* **2010**, *35*, 7667-7674.

(48) Shen, C.; Chen, H. M.; Qiu, M. Y.; Shi, Y. Q.; Yan, W.; Jiang, Q. R.; Jiang, Y. Q.; Xie, Z. X. Introducing Oxophilic Metal and Interstitial Hydrogen into the Pd Lattice to Boost Electrochemical Performance for Alkaline Ethanol Oxidation. *J. Mater. Chem. A* **2022**, *10*, 1735-1741.

(49) Pan, Y.; Li, H. D.; Wang, Z. C.; Han, Y.; Wu, Z. C.; Zhang, X. T.; Lai, J. P.; Wang, L.; Feng, S. H. High-efficiency Methanol Oxidation Electrocatalysts Realized by Ultrathin PtRuM-O (M = Ni, Fe, Co) Nanosheets. *Chem. Commun.* **2020**, *56*, 9028-9031.

(50) Saha, S.; Gayen, P.; Wang, Z. Y.; Dixit, R. J.; Sharma, K.; Basu, S.; Ramani, V.K.; Development of Bimetallic PdNi Electrocatalysts toward Mitigation of Catalyst Poisoning in Direct Borohydride Fuel Cells. *ACS Catal.* **2021**, *11*, 8417-8430.

(51) Yang, X. B.; Wang, Q.; Qing, S. J.; Gao, Z.; Tong, X. L.; Yang, N. J. Modulating Electronic Structure of an Au-nanorod-core-PdPt-alloy-shell Catalyst for Efficient Alcohol Electro-Oxidation. *Adv. Funct. Mater.* **2021**, *11*, 2100812.

(52) Nurdan, C.; Ahmet, B.; Mehmet, Y.; Efecan, E. I.; Hilal, K.; Murat, K.; Mehmet, Z. Atomic Layer Deposition-SiO_2 Layers Protected PdCoNi Nanoparticles Supported on TiO_2 Nanopowders:

Exceptionally Stable Nanocatalyst for the Dehydrogenation of Formic Acid. *Appl. Catal. B Environ.* **2017**, *210*, 470-483.

(53) Zhang, L. L.; Ding, L. X.; Chen, H. B.; Li, D. D.; Wang, S. Q.; Wang, H. H. Self-supported PtAuP Alloy Nanotube Arrays with Enhanced Activity and Stability for Methanol Electro-Oxidation. *Small* **2017**, *13*, 1604000.

(54) Liu, Z. L.; Ling, X. Y.; Su, X. D.; Lee, J. Y. Carbon-Supported Pt and PtRu Nanoparticles as Catalysts for a Direct Methanol Fuel Cell. *J. Phys. Chem. B* **2004**, *108*, 24, 8234-8240.

(55) Tiwari, J. N.; Pan, F. M.; Lin, K. L. Facile Approach to the Synthesis of 3D Platinum Nanoflowers and their Electrochemical Characteristics. *New J. Chem.* **2009**, *33*, 1482-1485.

(56) Koenigsmann, C.; Wong, S. One-dimensional Noble Metal Electrocatalysts: a Promising Structural Paradigm for Direct Methanolfuelcells. *Energy Environ. Sci.* **2011**, *4*, 1161-1176.

(57) Scofield, M. E.; Koenigsmann, C.; Wang, L.; Liu, H. Q.; Wong, S. S. Tailoring the Composition of Ultrathin, Ternary Alloy PtRuFe Nanowires for the Methanol Oxidation Reaction and Formic Acid Oxidation Reaction. *Energy Environ. Sci*. **2015**, *8*, 350-363.

(58) Li, J. S.; Luo, Z. S.; He, F.; Zuo, Y.; Zhang, C. Q.; Liu, J. F.; Yu, X. T.; Du, R. F.; Zhang, T.; Infante-Carrio, M. F.; Tang, P. Y.; Arbiol, J.; Llorca, J.; Cabot, A. Colloidal Ni-Co-Sn Nanoparticles as Efficient Electrocatalysts for the Methanol Oxidation Reaction, *J. Mater. Chem. A* **2018**, *6*, 22915-22924.

(59) Lin, B. Q.; Wu, X.; Xie, L.; Kang, Y. Q.; Du, H. D.; Kang, F. Y.; Li, J.; Gan, L. Atomic Imaging of Subsurface Interstitial Hydrogen and Insights into Surface Reactivity of Palladium Hydrides. *Angew. Chem. Int. Ed.* **2020**, *59*, 20348-20352.

(60) Zan, G. T.; Wu, T.; Zhang, Z. L.; Li, J.; Zhou, J. C.; Zhu, F.; Chen, H. X.; Wen, M.; Yang, X. C.; Peng, X. J.; Chen, J.; Wu, Q. S. Bioinspired Nanocomposites with Self-adaptive Stress Dispersion for Super-Foldable Electrodes. *Adv. Sci.* **2022**, *9*, 2103714.

Table of Contents

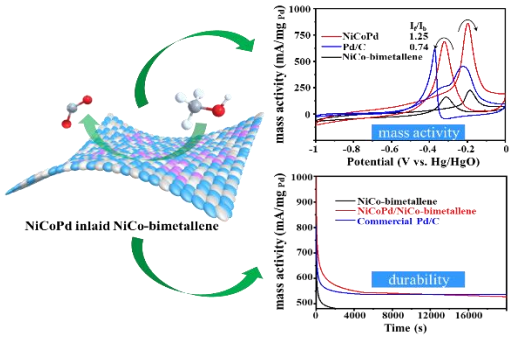

NiCoPd inlaid NiCo-bimetallene, which is synthesized firstly by structure directing effect of 18-crown-6 ether at the interface of two-phase solution together with HCHO reduction and atom-diffusion-aging process, exhibits excellent mass activity and anti-CO poisoning ability for MOR.